Int J Adv Manuf Technol (2018) 95:2015–2025
https://doi.org/10.1007/s00170-017-1248-3

ORIGINAL ARTICLE

Investigation on the creep-age forming of an integrally-stiffened AA2219 alloy plate: experiment and modeling

Youliang Yang[1] · Lihua Zhan[1,2,3] · Rulin Shen[1] · Jian Liu[1] · Xicai Li[1] · Minghui Huang[1,2,3] · Diqiu He[1,2,3] · Zhilong Chang[4] · Yunlong Ma[4] · Li Wan[5]

Received: 12 April 2017 / Accepted: 24 October 2017 / Published online: 18 November 2017

Abstract Creep-age forming (CAF) is a relatively new sheet metal forming method for manufacturing large-scale components with accurate shape and desired performance. This paper fully investigates the strain distribution, springback characteristic, mechanical property, and shape quality of an integrally-stiffened AA2219 alloy plate during CAF process. A new set of unified creep-ageing constitutive equations incorporating the effect of pre-deformation is developed, and its effectiveness in FE solver MSC.Marc is validated by tension creep-ageing simulation. CAF simulation of the stiffened plate is conducted. The results indicate that the final shape of the plate is simultaneously determined by plastic and creep deformations, while the creep deformation plays a major role, with corresponding contribution percentage of 33 and 67%. Comparisons between experiment and modelling show that the deviations are approximately 11% for springback and 3.2% for yield strength, which confirms the validity of CAF modelling. Furthermore, yield strengths on the skin of the plate are more evenly distributed as compared with those on the stiffeners. In addition, the values of generatrix linearity of the formed plate are very small, which demonstrates that the CAF-formed integrally-stiffened plate has high-precision shape quality.

Keywords Creep-age forming · Integrally-stiffened plate · Modeling · Springback · Mechanical property · Shape quality

✉ Lihua Zhan
yjs-cast@csu.edu.cn

[1] College of Mechanical and Electrical Engineering, Central South University, Changsha 410083, China

[2] State Key Laboratory of High-Performance Complex Manufacturing, Central South University, Changsha 410083, China

[3] Nonferrous Metal Oriented Advanced Structural Materials and Manufacturing Cooperative Innovation Center, Central South University, Changsha 410083, China

[4] Beijing Institute of Astronautical Systems Engineering, Beijing 10007, China

[5] Capital Aerospace Machinery Company, Beijing 100076, China

1 Introduction

With the development of aeronautics and astronautics, large integral panel components have been widely used in civil and military aircrafts, space crafts, and launch vehicles [1]. Typically, panel component is assembled by riveting the stringers/ribs and skin, which is also called built-up structure. For integral structure, the stringers/ribs are machined out of a thick plate by CNC machine [2]. In contrast, the integral structure has the advantages as follows: (1) its geometric configuration can be designed with very complex spatial surfaces, satisfying harsh aerodynamic requirements; (2) the use of fillet transition between the skin and stringers/ribs can effectively reduce the stress concentration; (3) the weight and manufacturing cost can be reduced greatly [3]. However, traditional forming methods have been proved to be inadequate for producing large integral components, as formed parts cannot remain stable in dimension and often suffer micro cracks.

Creep-age forming (CAF) is a relatively new metal forming process for manufacturing large-scale lightweight components with high level of performance. CAF is composed of stress relaxation and artificial aging, which are respectively responsible for forming and strengthening materials. In a CAF process, part to be formed is pressed completely onto the tool's surface by extracting the air between vacuum bagging film and mold. The part is then heated for a pre-selected amount of time sufficient for stress relaxation and creep. Finally, the

part is released from the tool and springbacks due to elastic recovery [4, 5]. Several constitutive equations have been proposed to predict creep deformation behavior or springback of material. Sallah et al. [6] presented a simplified inelastic constitutive equation for autoclave age forming using a cylindrical tool shape and a good agreement was obtained between the predictions and Textron data. Kowalewski et al. [7] derived a mechanism-based constitutive equation with three internal state variables, which could model the primary, secondary and tertiary creeps. As microstructural evolution theory developed, constitutive equations are more comprehensively established by incorporating the interactions of precipitate nucleation and growth, dislocation density, mechanical properties, and creep deformation [8–11].

So far, successful applications of CAF include the upper wing skins of Gulfstream GIV, B-1B long-range combat aircraft, and Airbus A330/340/380 [1, 12]. However, most of these components are panel-shaped. A few attempts have been made concerning the creep-age forming of integrally-stiffened plate. Adachi et al. [2] studied the CAF of a lower wing with stringer structure. They established an analytical model to predict the amount of springback through introducing a parameter of CAF equivalent modulus. CAF test was carried out on AA7475 lower wing panel, revealing that the maximum difference between the experimental and predicted values was approximately 7%. Based on the classical plate bending theory, Inforzato et al. [13] employed the concept of equivalent height to simplify the geometry of complex stiffened panel, which enabled the springback magnitude of creep-age-formed part to be estimated easily. They found that the calculated springback was very close to the average value measured in the part. Lam et al. [14] developed a novel forming technique, which made use of PTFE pocket fillers and intermediate sheets to reinforce and protect stiffeners during CAF process, to research the effects of different stiffener designs and preform age conditions on springback of formed part.

AA2219 is extensively used in aerospace industries due to its excellent weldability, good high-and-low temperature performance. Our previous research [15, 16] shows that 7% stretching of 2219 aluminum alloy between solution treatment and creep aging can simultaneously improve shape precision and mechanical properties of creep-age-formed plate. The aim of this paper is to study the forming characteristics of 7% predeformed AA2219 plate with stiffeners by methods of experiment and modeling. A new set of creep-aging constitutive equations which considers the effect of pre-deformation is developed and its effectiveness in FE solver MSC.Marc is validated by tension creep-aging simulation. Then CAF simulation of the stiffened plate is performed. Strain distribution, springback behavior, mechanical property, and shape quality of the integrally-stiffened plate are fully analyzed. Furthermore, CAF experiment of the stiffened plate is conducted and the experimental and simulation results are compared.

2 Constitutive and numerical modeling

2.1 Unified creep-aging constitutive modeling

The unified creep-aging constitutive model is derived based on microstructural state variable approach, relating material responses to microstructural state variables [15]. During creep aging, the variation of precipitates is described by average length (l), aspect ratio (q), and normalized volume fraction ($\overline{f_v}$), which take the effect of dislocation density (ρ) into account. The following set of equations is established:

$$\begin{cases} \dot{l} = C_2 \cdot (a + b \cdot \sigma - l)^{m_3} \cdot \left(1 + k_3 \cdot \bar{\rho}^{n_4}\right) \\ q = C_3 \cdot exp\left[-k_4 \left(t - t^*\right)^2 - \sigma^{n_5}\right] \cdot t^{n_6} + 1 \\ \dot{\overline{f_v}} = \dfrac{C_1 \cdot l^3 \cdot \dot{l}}{q} \left(1 - \overline{f_v}\right)^{m_2} \cdot (1 + k_2 \cdot \bar{\rho}^{n_3}) \\ \dot{\bar{\rho}} = -C_4 \cdot \bar{\rho} \cdot \left|\dot{\varepsilon_c}\right| \end{cases} \tag{1}$$

where C_1, C_2, C_3, C_4, m_2, m_3, n_3, n_4, n_5, n_6, a, b, k_2, k_3, k_4, and t^* are material constants. The l, q and $\overline{f_v}$ are obtained by statistical analysis of TEM photos. The term $(a + b \cdot \sigma)$ represents the peak value of average length of precipitate under varying applied stresses (σ). The t and t^* respectively denote current and peak-aging time of material. Material constants a, b, and t^* can be measured experimentally. The normalized dislocation density ($\overline{\rho}$) is defined as $\overline{\rho} = \rho/\rho_m$ with ρ and ρ_m being current and maximum dislocation density of material, respectively. Li et al. [17] claimed that there is a limit of the pre-stretch level, above which the age hardening progress would be hardly affected by further increasing pre-stretch levels. For the Al–2.45Cu–2.45Li alloy, the limit is about 6%. For AA2219 in this study, the 7% pre-stretch in initial temper may have reached the limit level and thus the initial dislocation density can be supposed to be saturated state. During creep aging, under the action of high temperature thermal activation and high stress, the saturated dislocations are prone to annihilate and dynamically recover. So the normalized dislocation density rate is formulated as a decreasing trend. The yield strength (σ_y) of age-hardenable aluminum alloy has contributions from the intrinsic strength (σ_i), solid solution hardening (σ_{ss}), precipitation hardening (σ_{ppt}), and dislocation hardening (σ_{dis}). The intrinsic strength, which may include strengthening components from dispersoids and grain size, is considered constant [18]. And the latter three components are associated with microstructural state variables, which are expressed as follows:

$$\begin{cases} \sigma_y = \sigma_i + \sigma_{ss} + \sigma_{ppt} + \sigma_{dis} \\ \sigma_{ss} = C_{ss} \cdot \left(1 - \overline{f_v}\right)^{2/3} \\ \sigma_{ppt} = c_{ppt} \cdot \overline{f_v}^{1/2} \cdot q^{n_1} \\ \sigma_{dis} = C_{dis} \cdot \overline{\rho}^{n_2} \end{cases} \tag{2}$$

where C_{ss}, C_{ppt}, C_{dis}, n_1, and n_2 are material constants. With creep-aging time, the concentration of solute atoms and dislocation density gradually decrease, leading to reduction in solute hardening (σ_{ss}) and dislocation hardening (σ_{dis}). The aspect ratio (q), which increases until peak age and then decreases [19], is added in the precipitation hardening (σ_{ppt}) equation to characterize the mechanisms of dislocation cutting and bypassing. The creep strain rate is not only a function of applied stress (σ) but also the function of yield strength (σ_y):

$$\dot{\varepsilon_c} = A \cdot sinh\left\{\frac{B\cdot(\sigma-\sigma_0)\cdot(1+k_1\bar{\rho})}{\sigma_y}\right\}^{m_1} \quad (3)$$

where A, B, k_1, and m_1 are material constants. σ_0 is threshold stress of creep. In the case of $\sigma \geq \sigma_0$, creep strain occurs, and vice versa. Pre-deformation exerted on aluminum alloy before creep-age process provides massive moveable dislocation, which promotes creep deformation [15, 20]. Here, a positive effect of mobile dislocation on creep strain rate is considered.

Combining Eqs. (1), (2), and (3), we obtain the unified creep-aging constitutive model which can describe creep deformation and yield strength of material simultaneously during CAF process. Constant tensile stress creep-aging tests are carried out using 7% pre-deformed AA2219 test-pieces, at the temperature of 165 °C and at stress levels of 120, 150, and 180 MPa for 11 h (peak-aging time of the tested 2219 aluminum alloy). Material constants within the model are calibrated from experimental data and listed in Table 1. More detailed description of the constitutive equations can be referred to [15].

To validate the effectiveness of the developed creep-aging constitutive model in the FE solver MSC.MARC, the FE model of the tensile creep test at 165 °C for 2219 aluminum alloy is established and shown in Fig. 1a. The constitutive model is programmed by FORTRAN language and implemented in the FE solver by user defined subroutine, CRPLAW. In terms of creep strain and yield strength, the comparisons between experimental and computed results are conducted to verify the above model, as depicted in Fig. 1b and c. Obviously, the experimental data agrees well with simulated results. This illustrates that the constitutive model can accurately predict the creep-age behavior of 2219 aluminum alloy in FE solver.

2.2 FE modeling

Figure 2 shows the FE model for CAF process of an integrally-stiffened plate using MSC.Marc. The geometric dimension of the plate is shown in Fig. 3. The plate is modeled as 3D deformable shell element with the simplification of removing hole and fillet features. Three-node triangular shell element is used at the skin area of the plate. While the two ends and stiffeners of the plate are meshed by using four-node quadrilateral shell element, so that the skin area and stiffeners of plate could share the same nodes at the intersections. The tool surface of 1160-mm radius is set as rigid body. Four springs at the corners are used to support the weight of the plate and to separate the plate from the mold at the end of simulation. Young's modulus of 67.552 GPa and Poisson's ratio of 0.3 are assigned for the studied AA2219 and the room-temperature engineering stress-strain behavior of the material shown in Fig. 4 is imported into the model. The verified subroutine, CRPLAW, is implemented to model the creep-aging process of the integral plate. The symmetric boundary conditions are defined on nodes along the dotted lines in Fig. 2. And the bottom node of each spring is completely constrained.

Simulation process can be divided into three steps. Initially, the pressure is incrementally applied on the upper surface of the plate until it reaches 0.45 MPa, under which the plate is fully contacting with the surface of mold. Subsequently, this load is kept for 8 h to allow the creep deformation and age hardening to take place. Last the pressure is released and the surface data of the simulated plate is obtained.

3 Experimental

3.1 Materials

The raw material, AA2219 plate of 1900 mm × 1000 mm × 20 mm, was provided by a company. The as-received material was in a T37 temper which had undergone solution heat-treatment at 535 °C for 80 min, water-quenching, followed by 7% pre-stretching. The chemical

Table 1 Material constants of pre-deformed AA2219 at 165 °C

$A(h^{-1})$	B	$\sigma_0(MPa)$	$\sigma_i(MPa)$	$C_{ss}(MPa)$	$C_{ppt}(MPa)$	$C_{dis}(MPa)$	C_1	C_2	C_3	C_4	k_1	k_2	k_3
0.95	0.14	15.4	111.2	70.3	79.1	125.1	3.7e-6	1.0	141.9	271.8	1.63	0.38	0.56
$k_4(h^{-2})$	n_1	n_2	n_3	n_4	n_5	n_6	m_1	m_2	m_3	$a(nm)$	$b(nm/MPa)$		$t^*(h)$
0.01	0.22	0.05	5.0	4.68	0.17	0.1	3.2	0.55	0.60	94.0	− 0.1		11

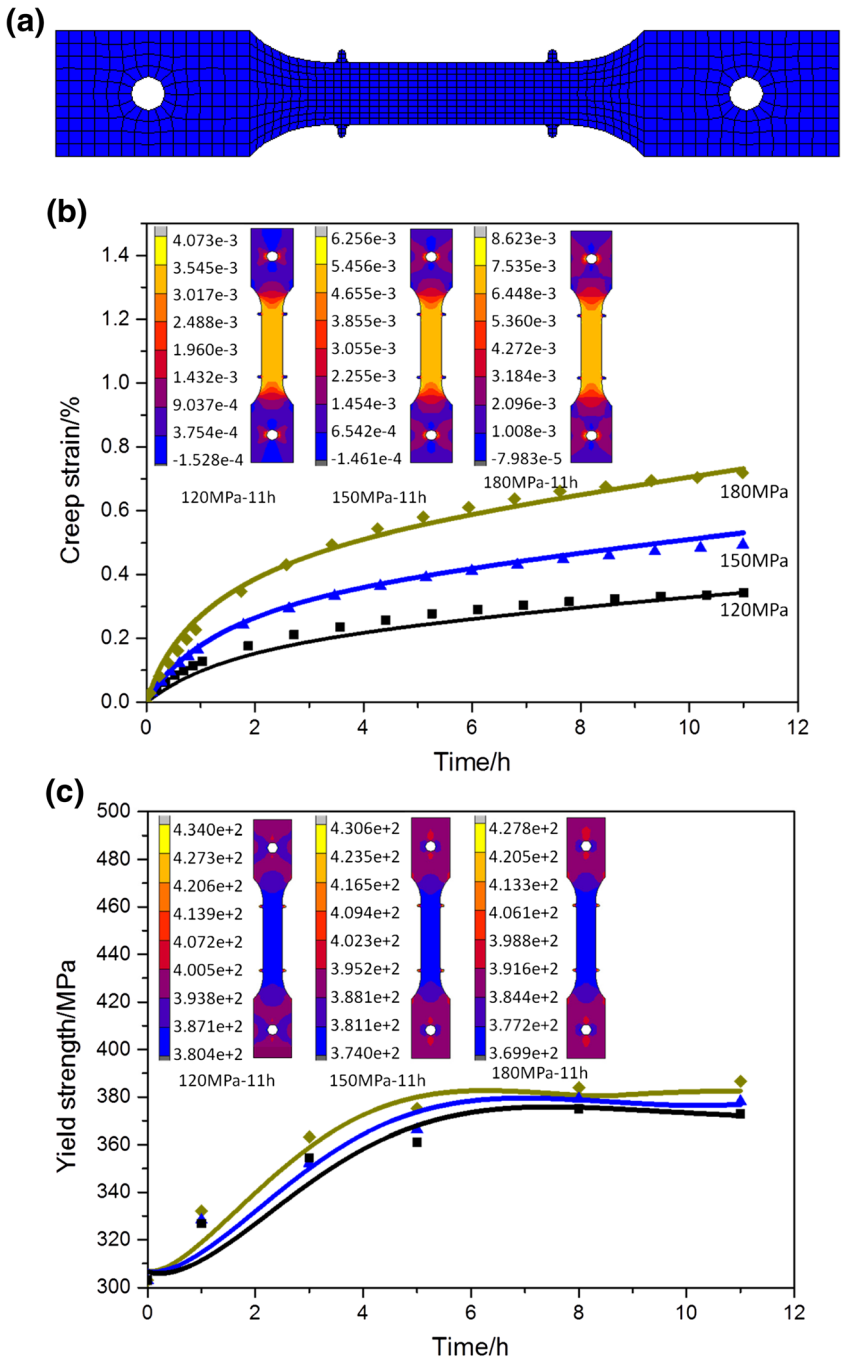

Fig. 1 Comparisons between experimental and computed results of tensile creep tests at 165 °C. **a** FE model of tensile creep test. **b** Creep strain. **c** Yield strength. Symbols and solid lines denote experimental data and computed curves, respectively.

compositions of AA2219 are given in Table 2. The integrally-stiffened plate in Fig. 3 were machined parallel to the rolling direction of as-received plate. A laboratory autoclave was used in this study, and the temperature and pressure in the autoclave are controlled by PID system with the accuracy of ± 1.5 °C and ± 0.01 MPa. The Atos Raster Scanner was used to scan the outer shape of the formed plate, and the mechanical properties were measured by an INSTRON 5500 machine.

3.2 Experimental method

The CAF test is split into three operations: loading, creep-aging, and unloading. The specific experimental procedure can be described as follows:

- Loading (Fig. 5a). The mold and plate were wrapped by breather and then sealed by vacuum bagging film. And the air in the assembly was extracted by vacuum pump.

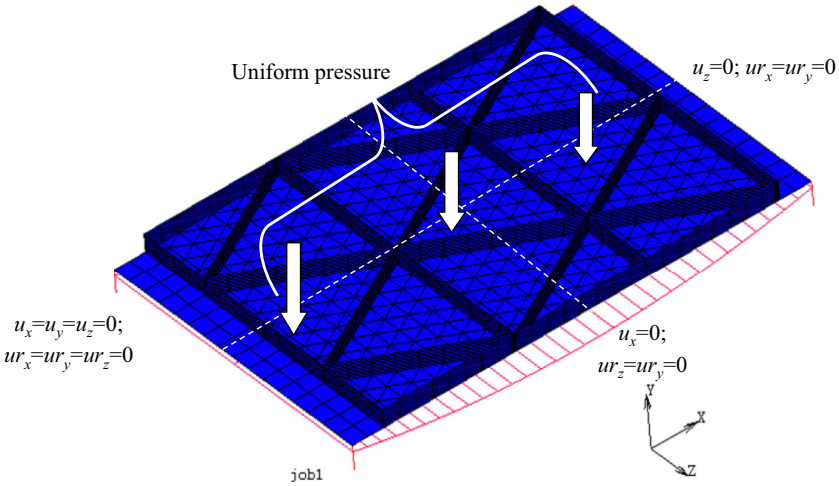

Fig. 2 FE model with the boundary conditions

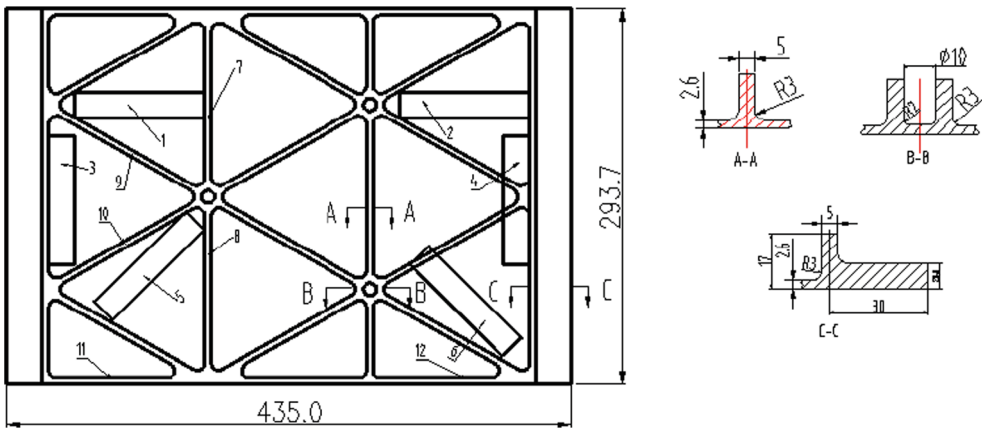

Fig. 3 Dimensions of the integrally-stiffened plate (units in mm)

- Creep-aging (Fig. 5b). The sealed mold was sent into the autoclave. Two thermocouples were mounted in the middle and end of the mold, respectively. The process parameters were aging temperature of 165 °C, holding time of 8 h and applied pressure of 0.45 MPa.

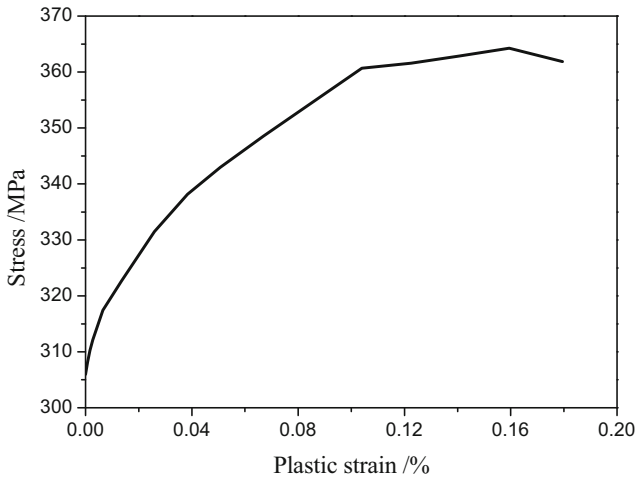

Fig. 4 Room-temperature engineering stress-strain behavior of AA2219

- Unloading (Fig. 5c). After holding time, the furnace was ventilated to allow the apparatus to return to room temperature.

4 Results and discussion

4.1 Strain distribution

Figure 6 displays the final equivalent plastic and creep strain distributions of the plate after CAF process. In Fig. 6a, plastic strains are generated in the stiffeners of plate and maximum equivalent plastic strain reaches 1.208e-2. It is evident that most plastic strains are accumulated within the ring and sideling stiffeners at the middle region of the plate (inside green box). But plastic strains are barely seen in the axial stiffeners

Table 2 Chemical compositions of AA2219 (mass fraction, %)

Cu	Mg	Mn	Si	Fe	Ni	Zr	Ti	Al
5.24	0.028	0.27	0.042	0.13	0.03	0.14	0.065	Bal.

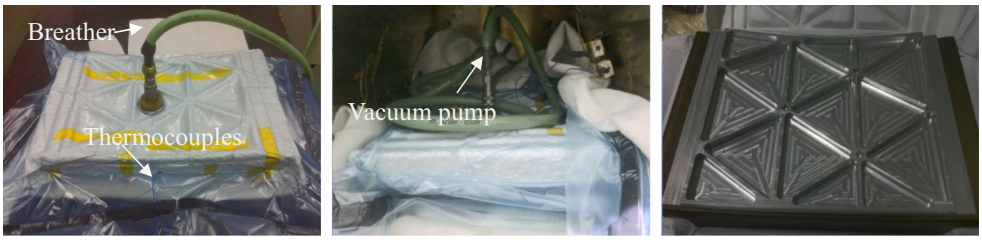

Fig. 5 Creep-age forming of the stiffened plate

and skin. From Fig. 6b, creep strains are distributed in most regions of the ring and sideling stiffeners. This is because the initial stress levels of these stiffeners caused by loading are higher than other structures, as shown in Fig. 7, and higher initial stress level results in larger creep strain [11]. For the sake of contrastive analysis, feature nodes at the top of stiffener (No. 1958) and on the skin (No. 188) are chosen shown in Fig. 7. The variation of equivalent von Mises stress of two nodes during the creep aging stage is plotted in Fig. 8. Referring to Fig. 8, the stress of stiffener node 1958 is relaxed gradually with creep-aging time by 134.6 MPa. Accordingly, part of elastic deformation on the stiffener is converted into creep deformation. While for skin node 188, the initial stress level is 8.2 MPa lower than creep threshold stress in Eq. (3); thus, creep deformation does not occur. According to the above analysis, creep strains are distributed in most regions of the ring and sideling stiffeners. Note that stress of skin node 188 is decreased first and then increased for a long time. The decrease in stress at initial stage may be due to the softening caused by thermal activation role. With extension of time, the stress is increased as a result of precipitation hardening. Referring to Fig. 6, there is almost neither plastic nor creep

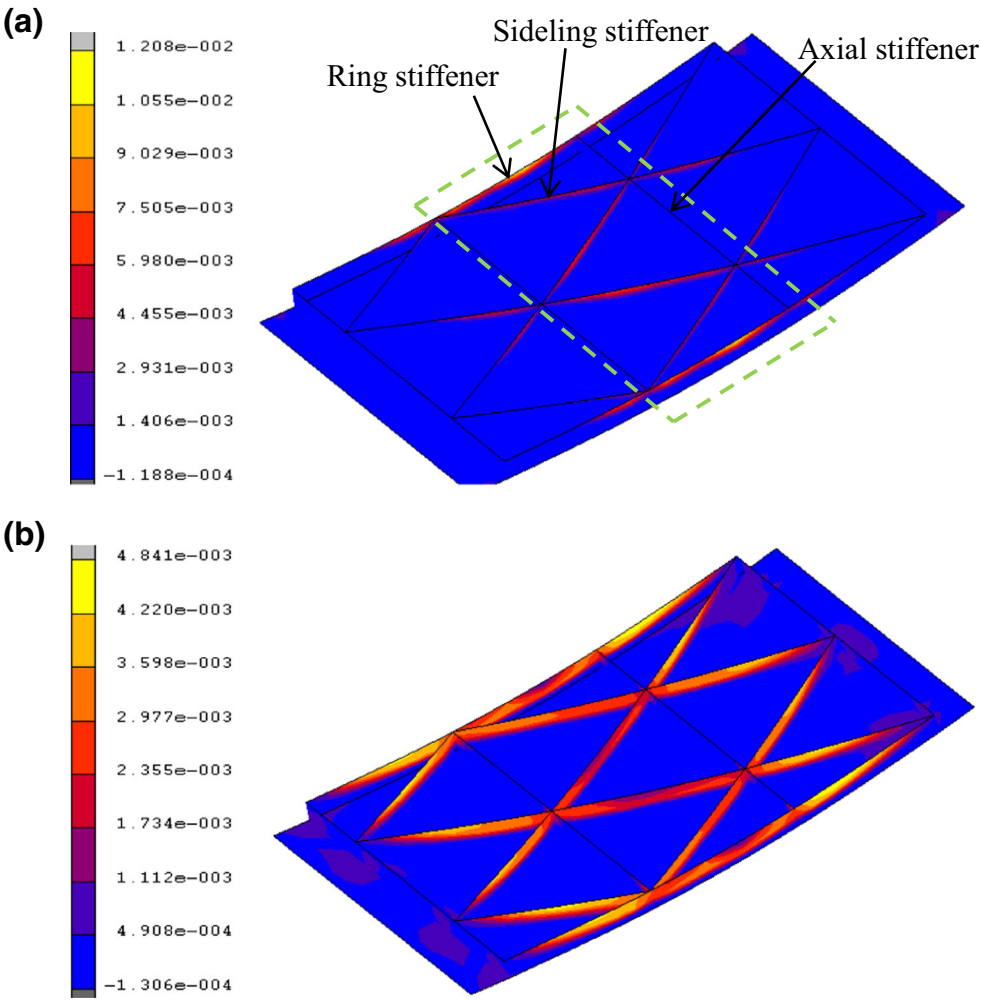

Fig. 6 Final equivalent strain distributions of plate. **a** Plastic strain distribution. **b** Creep strain distribution

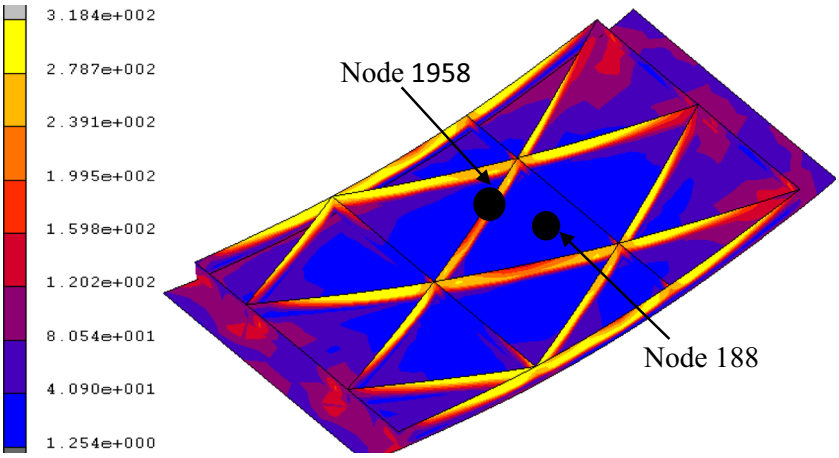

Fig. 7 Equivalent von Mises stress distribution of plate after loading

strain occurred in the axial stiffener. This is due to the fact that the curvature direction of the tool is perpendicular to the axial stiffeners, which results in low stress levels and ultralow strain [21]. It demonstrates that the deformation of plate is associated with the direction of stiffener distribution. To sum up, the stiffeners have plastic and creep strains synchronously while the skin just has a few creep strains. It further reveals that the final shape of plate contributes from plastic and creep strains, and the stiffeners play a major role. Specifically, the contributions of plastic and creep deformations account for the proportion of 33 and 67%, respectively.

4.2 Springback behavior

The magnitude of plate's springback is represented by $SP = (1 - R_o/R_f) \times 100\%$, where R_o and R_f are the outer surface radii of the plate before and after the load is released. The smaller the SP value is, the more accurate the formed plate is. The outer surface radius values of experimental and simulated plates are measured as 1308.5 and 1500.0 mm, and corresponding springback values 11.3 and 22.7%. By comparison, it can be seen that springback deviation between experimental and simulated plates reaches up to 11%. The following two influencing factors mainly lead to the above deviation. During CAF of stiffened plate, it is found that it takes about 5 h for plate's temperature to increase from room to aging temperature, as illustrated in Fig. 9. However, during the temperature rising period, lots of creep deformations take place. Creep deformation curve of AA2219 test-sample imitating the temperature-rise process of plate is shown in Fig. 10. It can be observed that the creep deformation during the temperature rising period accounts for a total creep deformation of approximately 25%. Therefore, heating process of plate should be considered in the CAF simulation to improve the prediction accuracy of springback. It is well known that during the creep aging forming process, there are simultaneous tensile and compressive stresses inside the component. Li et al. [17] and Xu et al. [22] found that under the same conditions, the tensile stress creep deformation would be greater than the compressive stress creep deformation. In this paper, the parameters in

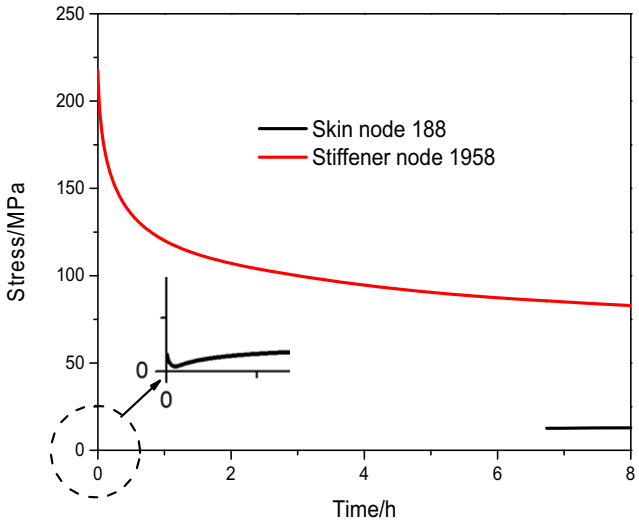

Fig. 8 Stress variation curves of the stiffener and skin nodes

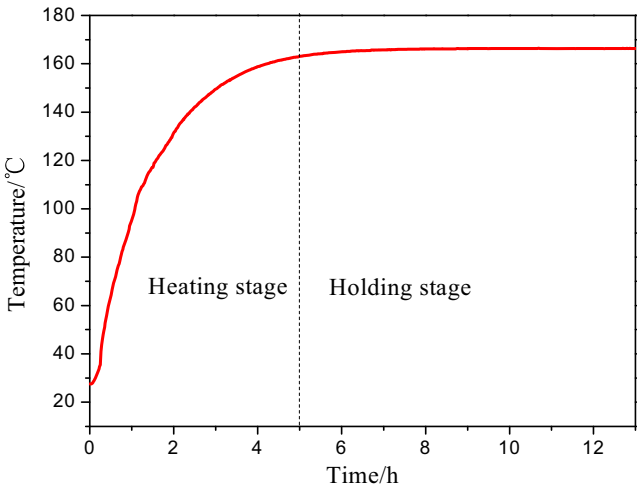

Fig. 9 Temperature change curve of the plate during CAF process

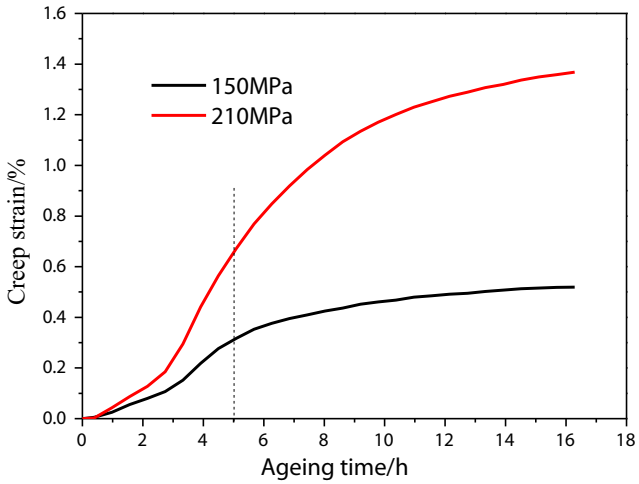

Fig. 10 Creep deformation curve of AA2219 sample simulating the temperature-rise process of plate

the constitutive model are identified using experimental data of tensile stress creep aging. As a consequence, in the CAF simulation of plate, compressive stress creep deformation computed by FE model are larger than that of practical value, leading to more creep deformation generated in the plate and less springback.

4.3 Mechanical property

Figure 11 is the simulation result of yield strength of the plate after CAF process. On the whole, yield strength varies remarkably from the skin to stiffeners. Detailed values of yield strength at different positions (Fig. 3) of the simulated plate are tabulated in Table 3. Each value takes average of two specimens. As seen in Table 3, yield strengths on the skin are more uniformly distributed as compared with those on the stiffeners, which can be also proven by the lower value

Table 3 Simulation values of yield strength at different locations of the workpiece

Location	Skin			Stiffeners		
	0°	45°	90°	Axial	Ring	sideling
Yield strength (MPa)	401	400.8	392.7	413	385	378
Average strength (MPa)/ standard deviation	398.2/4.7			392/18.5		

of standard deviation. When the plate is completely pressed against the mold surface, the initial stress gradient along the skin thickness is small. That means there is no significant stress difference through the skin thickness. Moreover, it can be known that yield strength is related to initial stress according to the constitutive equations. Consequently, the skin has relatively uniform yield strength. For diverse types of stiffener, however, stress levels through the height change considerably. For example, stresses on the axial stiffeners remain slight during loading; but for the ring/sideling stiffeners, the stress levels constantly increase. This big stress difference between them leads to large deviation of yield strength. After loading, the stress increases from the axial ribs, skin, and other ribs. Due to the inverse, the axial ribs have largest strength and other ribs (ring and sideling ribs) are the weakest area in the formed plate. Mean values of yield strength on the skin are higher than those on the stiffeners (Table 3). Tensile samples of dimension shown in Fig. 12 are machined at the different locations from the experimentally formed plate (Fig. 3), and the room-temperature yield strengths are determined on all samples. The test results show that the average value of yield strength of the different positions is 382.9 MPa, which is lower by 3.2% than the finite element simulation results. This confirms the validity of CAF modeling.

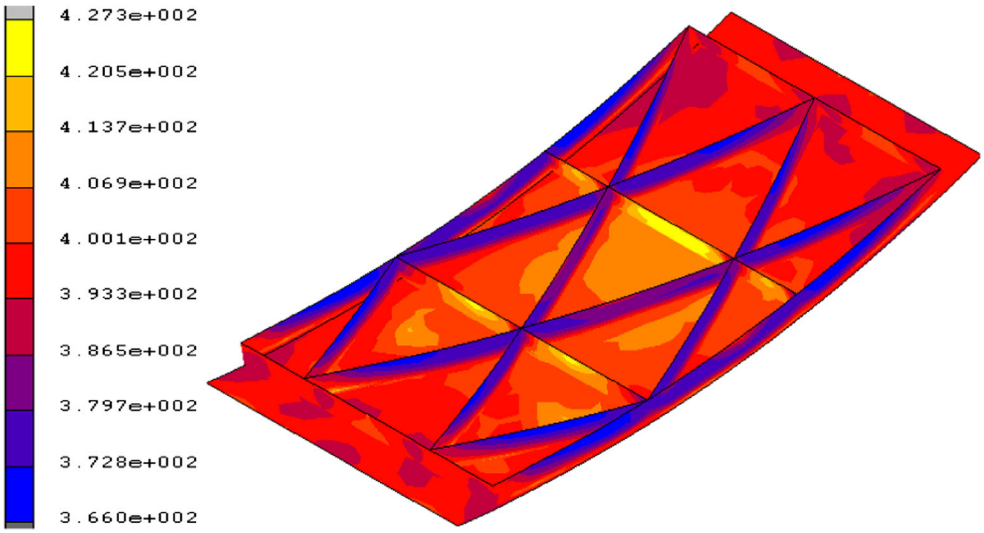

Fig. 11 Yield strength distribution of plate

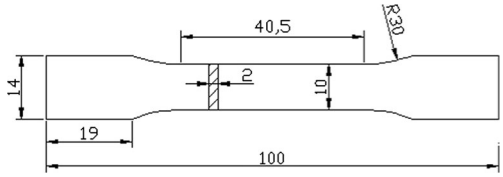

Fig. 12 Dimension of tension sample

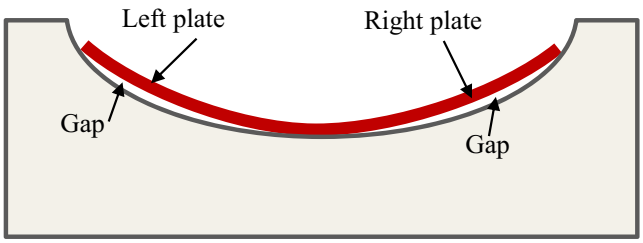

Fig. 14 Gaps between the plate and mold during CAF process

4.4 Shape quality

Figure 13 shows that the outer surface of the formed plate and fitted cylinder surface that was used to calculate plate's radius are not coincident. This illustrates that the deformation in plate's different areas are not uniform even though the mold is single curvature. The upper and lower regions of the plate are above fitted surface (see Fig. 13b) because the breather got caught in the space between the mold and plate in the process of vacuum-pumping, which also increases the tool surface radii of these two regions when compared to the middle area [16].

The initial flat plate approaches the mold surface gradually and slowly under pressure. However, when the bending plate nearly touches the tool's surface, the middle part of plate will first contact with the bottom surface, because the bending moment is larger. Under this situation, the two plates on the left and right sides bear insufficient bending moment to make them to touch the mold surface completely which leaves gaps between the plate and mold shown in Fig. 14. Although the applied pressure gradually increases, the gaps cannot vanish entirely. As a result, the left and right sides of the formed plate overtop the fitted surface, as shown in Fig. 13b.

Figure 15 shows the deflection distribution between outer surface of the formed plate and the initial flat plate. Due to the symmetry, five lines on the left side are used to evaluate the generatrix linearity of the formed plate. Specifically, the deflections of seven points on each line with intervals of 45 mm along *Y* axis direction are measured. It can be observed that at upper and lower edges of the plate, i.e., y = 11.5 and 281.5 mm, the deflections on the lines 2~5 are smaller than that of the middle area, which further proves that the breather got caught in the space during loading stage. The deflections on each line are evenly distributed and the maximum differences (generatrix linearity) are 0.18, 0.14, 0.32, 0.42, and 0.36 mm for line 1, 2, 3, 4, and 5, respectively. Normally, generatrix linearity of the integrally-stiffened plate manufacturing by roll-bending process method could reach up to about 3~4 mm [23]. By contrast, the integrally-stiffened plate possesses high geometric accuracy and deformation homogeneity after CAF process.

5 Conclusions

Creep-age forming of integrally-stiffened AA2219 plate was investigated under a single curvature bending radius of 1160 mm at for 8 h by experiment and modeling. The following conclusions can be drawn:

1. A new set of unified creep-aging constitutive equations considering the effect of pre-deformation is developed and then validated by tension creep-aging simulation.
2. Final shape of the integrally-stiffened plate contributes from plastic deformation and creep deformation concurrently, with corresponding percentages of 33 and 67%, respectively.
3. Comparisons between experiment and modeling show that the deviations are approximately 11% for springback and 3.2% for yield strength, which confirms the validity of CAF modeling. And yield strengths on the skin are more evenly distributed as compared with those on the stiffeners.

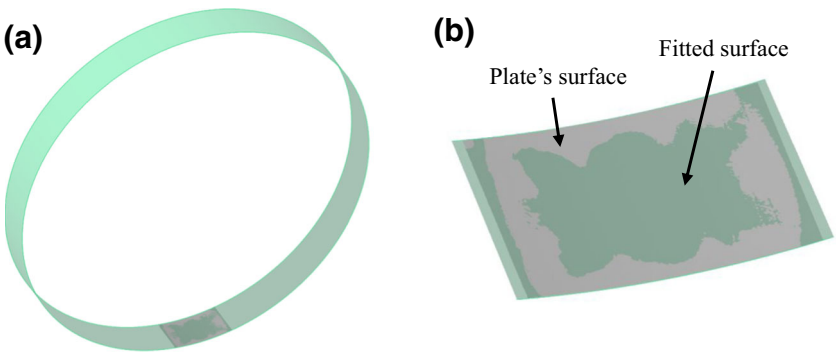

Fig. 13 Comparison of the outer surface of formed plate and fitted cylinder surface. **a** Overall diagram. **b** Magnification diagram

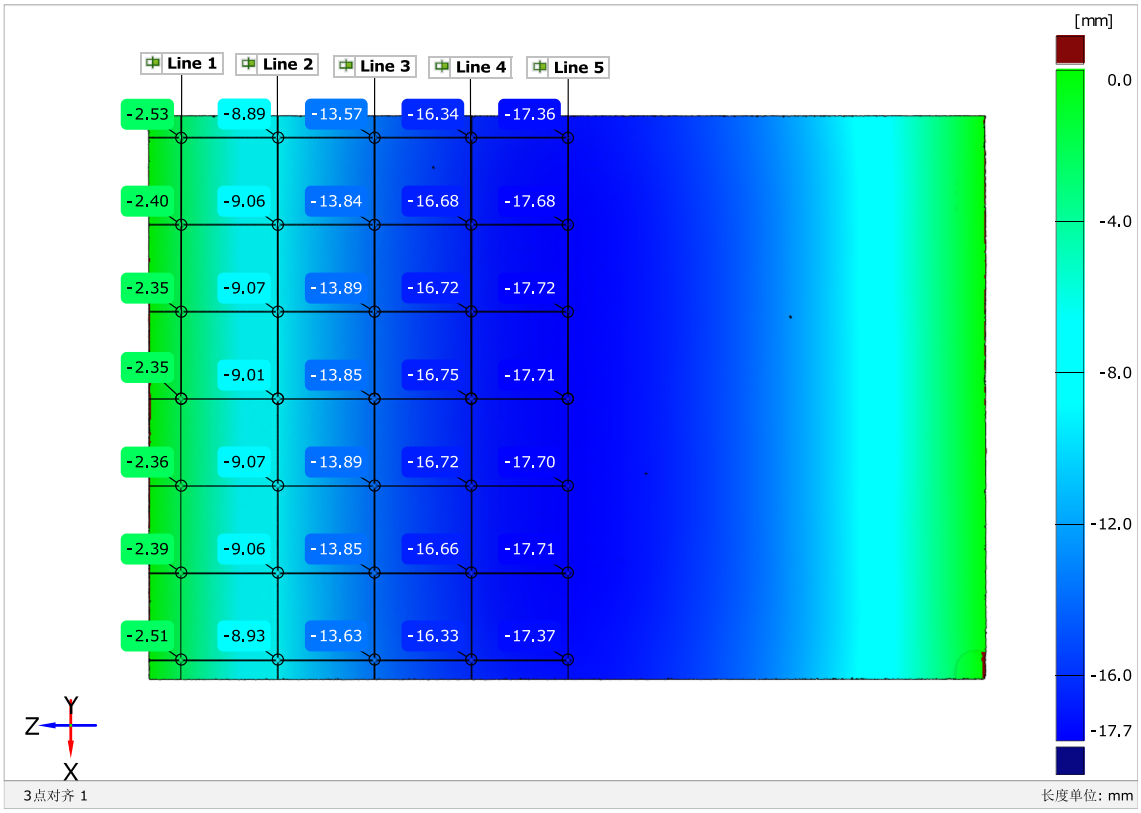

Fig. 15 Deflection distribution between outer surface of the formed plate and initial flat plate

4. Generatrix linearity of the formed plate is less than 0.5 mm, indicating that the integrally-stiffened plate possesses high geometric accuracy and deformation homogeneity after CAF process.

Funding information This research was supported by the National Basic Research Program of China (Grant No. 2014CB046602), the Key Program of National Natural Science Foundation of China (Grant No. 51235010), the Innovation-driven Project of Central South University (Grant No. 2015CX002), Specialized Research Fund for the Doctoral Program of Higher Education of China (Grant No. 20120162110003), and the Fundamental Research Funds for the Central Universities of Central South University (Grant No. 2017zzts090).

References

1. Zhan L, Lin J, Dean T (2011) A review of the development of creep age forming: experimentation, modeling and applications. Int J Mach Tools Manuf 51:1–17
2. Adachi T, Kimura S, Nagayama T (2004) Age forming technology for aircraft wing skin. Mater Forum 28:202–207
3. Zhan L, Yang Y (2016) Research on creep age forming technology for large integrated component. Aeron Manuf Technol 13:13–22
4. Brandão F, Delijaicov S, Bortolussi R (2017) CAF—a simplified approach to calculate springback in Al7050 alloys. Int J Adv Manuf Technol. https://doi.org/10.1007/s00170-016-9839-y
5. Khamneha M, Askari-Paykania M, Shahverdia H, Hadavib S, Emamia M (2016) Optimization of spring-back in creep age forming process of 7075 Al-Alclad alloy using D-optimal design of experiment method. Meas 88:278–286
6. Sallah M, Peddieson J, Foroudastan S (1991) Mathematical model of autoclave age forming. J Mater Process Technol 28:211–219
7. Kowalewski Z, Hayhurst D, Dyson B (1994) Mechanisms-based creep constitutive equations for an aluminium alloy. J Strain Anal Eng Des 29:306–316
8. Ho K, Lin J, Dean T (2004) Constitutive modelling of primary creep for age forming an aluminium alloy. J Mater Process Technol 153:122–127
9. Li C, Wan M, Wu X, Huang L (2010) Constitutive equations in creep of 7B04 aluminum alloys. Mater Sci Eng A 527:3623–3629
10. Zhang J, Deng Y, Zhang X (2013) Constitutive modeling for creep age forming of heat-treatable strengthening aluminum alloys containing plate or rod shaped precipitates. Mater Sci Eng A 563:8–15
11. Zhan L, Lin J, Huang M (2011) Experimental studies and constitutive modeling of the hardening of aluminum alloy 7055 under creep age forming conditions. Int J Mech Sci 53:595–605
12. Lam A, Shi Z, Lin J, Huang X, Zeng Y, Dean T (2015) A method for designing lightweight and flexible creep-age forming tools using mechanical splines and sparse controlling points. Int J Adv Manuf Technol. https://doi.org/10.1007/s00170-015-6982-9
13. Inforzato D, Costa P, Fernandez F, Travessa D (2012) Creep-age forming of AA7475 aluminum panels for aircraft lower wing skin application. Mater Res 15:596–602
14. Lam A, Shi Z, Yang H, Wan L, Davies C, Lin J, Zhou S (2015) Creep-age forming AA2219 plates with different stiffener designs and pre-form age conditions: experimental and finite elements studies. J Mater Process Technol 219:155–163
15. Yang Y, Zhan L, Shen R, Yin X, Li X, Li W, Huang M, He D (2017) Effect of pre-deformation on creep age forming of 2219 aluminum alloy: experimental and constitutive modeling. Mater Sci Eng A 683:227–235
16. Yang Y, Zhan L, Ma Q, Feng J, Li X (2016) Effect of pre-deformation on creep age forming of AA2219 plate: springback,

microstructures and mechanical properties. J Mater Process Technol 229:697–702
17. Li Y, Shi Z, Lin J, Yang H, Huang B, Chung T, Yang J (2016) Experimental investigation of tension and compression creep-ageing behaviour of AA2050 with different initial tempers. Mater Sci Eng A 657:299–308
18. Esmeili S, Lloyd D, Poole W (2003) A yield strength model for the Al-Mg-Si-Cu alloy AA6111. Acta Mater 51:2243–2257
19. Liu G, Zhang G, Ding X, Sun J, Chen K (2003) Modeling the strengthening response to aging process of heat-treatable aluminum alloys containing plate/disc- or rod/needle-shaped precipitates. Mater Sci Eng A 344:113–124
20. Xu Y, Zhan L, Li W (2017) Effect of pre-strain on creep aging behavior of 2524 aluminum alloy. J Alloys Compd 691(15):564–571
21. Luo h LW, Li C, Wan M (2017) Investigation of creep-age forming of aluminum lithium alloy stiffened panel with complex structures and variable curvature. Int J Adv Manuf Technol. https://doi.org/10.1007/s00170-017-0004-z
22. Xu Y, Zhan L, Xu L, Huang M (2017) Experimental research on creep aging behavior of Al-Cu-Mg alloy with tensile and compressive stresses. Mater Sci Eng A 682:54–62
23. Gao Y, Gong X, Hu L, Lei X (2017) Structure optimization and experimental verification on integral stiffened panel in roll-bending process. Forge Stamp Technol 42(6):66–69